Active Lifetime Extension for a 3L-NPC Inverter with Direct Torque Control

T. Minh Phan[1], H.A. Duy Nguyen[2], Mario Pacas[1]
Email: theminh.phan@uni-siegen.de; nhaduy@ctu.edu.vn; pacas@uni-siegen.de
[1] Professorship for Power Electronics and Electrical Drives, University of Siegen, Germany
[2] Can Tho University, Viet Nam

Abstract— **The redundant states in the output voltages of a Three-level Neutral Point Clamped Voltage Source Inverter (3L-NPC VSI) can be used to control the neutral point or to reduce the common mode voltage. However, the use of the redundant states to redistribute the losses among the switching devices of 3L-NPC VSI is a further possibility that was reported in previous papers. The proposed method for active redistribution of losses among the switching devices can become necessary in the practice to relieve stressed switches, which suffer excessive thermal stress due to malfunctions. In this paper, a new fault tolerant control approach is introduced to deal with this matter by modifying the switching table of the DTC (Direct Torque Control) scheme for a 3L-NPC VSI. An increased thermal stress in one IGBT module can be detected by sensing the temperature of the heatsink; consequently the switching patterns are immediately altered to redistribute the losses of the stressed IGBT module to the other cooler switches. Hence, the temperature of the stressed switches is kept under the critical limit and the thermal overload is reduced. In such way the reliability and the lifetime of inverter are maximized, even in case of thermal failure. This modulation scheme is called "Active Lifetime Extension" (ALE) and was presented in previous works for the case of field oriented control. In this paper the procedure is extended to the case of DTC.**

Keywords—Pulse width modulation, converter, semiconductor device reliability

I. INTRODUCTION

In high-power, medium-voltage applications, the semiconductor switches are often mounted on dedicated heatsinks; therefore there is no heat sharing among the switches. If one semiconductor device (Diode or IGBT) is exposed to excessive thermal stress, its lifespan is significantly reduced. The thermal overload of a semiconductor device during the operation of an inverter may occur due to degradation of the cooling system, to failures in firing or in the drivers, to inappropriate placing of the semiconductor devices, etc. In the following, a DTC scheme with a particular treatment of the pulse pattern is presented aiming at the reduction of the thermal stress of a particular semiconductor device by redistributing the losses to the other devices that are not affected by the failure. Because a thermal overload is avoided, a reduction of the lifetime of the affected semiconductor device is prevented.

The proposed strategy assumes that the temperature of each heatsink is monitored, thus the occurrence of a local thermal overload can be immediately detected. In case that the temperature of a semiconductor trespasses a threshold, the switching table of the DTC scheme is modified targeting a reduction of the losses in the overheated device by shifting the thermal load to the other semiconductors in the inverter that still have an efficient cooling function. The changes in the switching patterns that are necessary for this purpose should have a minimum impact on the quality of the inverter current quality and should not produce an excessive increase of the ripple of the neutral point voltage.

The control scheme proposed in this paper is explained for a Three-level Neutral Point Clamped Voltage Source Inverter (3L-NPC VSI) [1], but it is also applicable for any kind of multi-level inverter. Like other control methods that deal with similar issues the actively redistribution of the losses from the overloaded devices to the other cooler semiconductor switches makes use of the redundant states of the voltage space phasors. A main feature of the proposed control strategy is, as a long-term effect, the expected lifetime of the affected power semiconductors is significantly extended as the switching devices are protected against thermal overload [2]. Therefore this strategy was named ALE (active lifetime extension).

Several control methods that deal with the uniform distribution of the thermal load among the semiconductors in the 3L-NPC VSI are well-known. The objective of the proposals in [3][4][5] is a homogeneous distribution of the losses under normal operation of the 3L-NPC VSI. For this purpose, the topology of the inverter is modified by adding IGBTs parallel to the neutral point diodes to generate additional redundant states of switching states 0 (connection of one of the output phases to the neutral point). These extra states allow the desired uniform relocation of the losses. In the present work, the 3L-NPC VSI topology does not need any additional switches; only the control method and the switching patterns are adapted according to the thermal conditions in case of failure.

In [6] a different approach is presented, in which the redundancies of the zero voltage space phasors are also utilized for the redistribution of losses. The method presented there is restricted to the low modulation index range and to the operation with a load of reactive current. On the contrary the present work utilizes not only the zero voltage space phasors but also all the redundant states of voltage space phasors of the 3L-NPC VSI. Besides it can be applied for the whole voltage and current range of the inverter.

In previous works the ALE strategy had been realized by means of space vector modulation and was extensively investigated for the different operating points by means of simulation [7] as well as of experiments [8][9]. The results of these research works have shown that a significant reduction of the losses in the affected device can be achieved while keeping a

stable neutral point voltage, if the ALE method is properly applied. Based on the positive results in systems controlled by field-oriented schemes, the ALE strategy was further investigated for the case of DTC. As it will be shown in the following, the implementation effort of the ALE scheme is significantly reduced and the calculation of the switching patterns are simplified if compared with the former space vector modulation approach for 3L-NPC VSI.

The thermal measurements are time consuming and cumbersome, nevertheless numerous and comprehensive experiments were carried out on a downscaled (15kW) setup not only for the validation of the proposed control scheme but additionally to ensure the validity of simulation results. Therefore, the present work is based on reliable simulations of the examined system.

II. DTC FOR 3L-NPC INVERTER

A. Basic principle of DTC

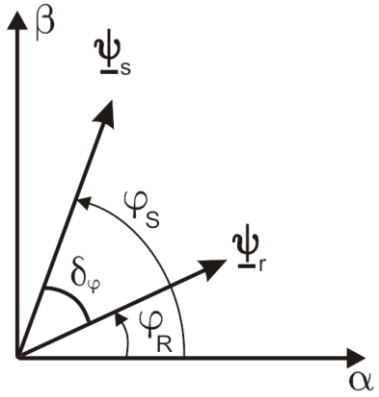

Fig. 1. Stator- and rotor-flux space phasors in the αβ-plane

While in Field Oriented Control (FOC) schemes the stator currents of the machine are the controlled variables, in DTC schemes the magnitude of the stator flux space phasor and the toque are the controlled variables [10]. Thus, one main equation is the relationship between the change of stator flux $\Delta\underline{\psi}_s$ space phasor and the stator voltage space phasor $\underline{u}_s$ of the induction machine as given by:

$$\frac{d\underline{\psi}_s}{dt} = (\underline{u}_s - R_s\underline{i}_s), \tag{1}$$

and can be simplified as

$$\Delta\underline{\psi}_s = (\underline{u}_s - R_s\underline{i}_s)\cdot\Delta t \approx \underline{u}_s\cdot\Delta t, \tag{2}$$

if the stator resistance R_s is small and can be neglected, Δt refers to the timespan while the stator voltage space phasor $\underline{u}_s$ is applied to the machine terminals. Based on this equation, the stator flux space phasor of the induction machine can be controlled by selecting the most appropriate one out of the different discrete voltage space phasors generated by the inverter. Besides, the electromagnetic torque T_i of the machine is calculated as:

$$T_i = k\cdot\left|\underline{\psi}_r\right|\cdot\left|\underline{\psi}_s\right|\cdot sin\delta_\varphi\ , \tag{3}$$

where the k is a proportionality factor, δ_φ is the angle between stator flux- $\underline{\psi}_s$ and rotor flux- $\underline{\psi}_r$ space phasors as shown in Fig. 1. Due to the large rotor time constant, for a short Δt the rotor flux space phasor can be considered virtually as fixed to the rotor. In contrast, the stator flux $\underline{\psi}_s$ can be rapidly changed as a function of the applied voltage according to equation (1). If an increase of torque is required, the voltage space phasor that causes the movement of $\underline{\psi}_s$ away of the $\underline{\psi}_r$ is chosen to increment the load angle δ_φ. Conversely, if a decrease of the torque is needed, the voltage space phasor should cause the reduction of the load angle δ_φ and is accordingly chosen. The control of the induction machine under a DTC scheme does not require either modulator or coordinate transformation and obviates the current controllers being very attractive because of its simplicity and higher dynamics.

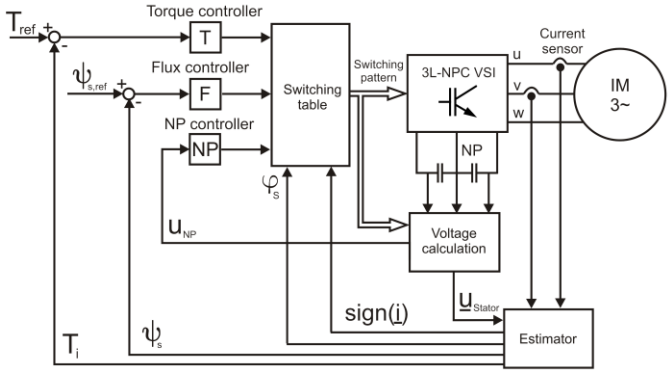

Fig. 2. Principal scheme of the DTC for an 3L-NPC VSI fed induction machine

B. DTC for a 3L-NPC VSI fed induction machine

Fig. 2 shows the principal DTC scheme for an induction machine (IM) fed by a 3L-NPC inverter. The controlled variables in this case are the torque T_i, the magnitude of the stator flux space phasor $\left|\underline{\psi}_s\right|$ and additionally the voltage of the middle point of the inverter U_{NP} (see Fig. 7). The actual values of torque T_i and of magnitude of the stator flux space phasor $\left|\underline{\psi}_s\right|$ are computed based on the measured currents and on the switching patterns together with the measured DC-link voltage. The ripple of the neutral point is measured and together with the actual values of T_i and of $\left|\underline{\psi}_s\right|$ are compared with their reference values by the hysteresis controllers to generate the switching pattern, so that the controlled variables are kept within their respectively predefined tolerance bands.

As the 3L-NPC VSI can generate 27 different switching states that correspond to the space phasor diagram in the α–β-plane with 12 sectors as depicted in Fig. 3, where the notation "–" refers to connection of one phase of inverter to the negative DC bus, "**0**" to neutral point, and "+" to the positive DC rail. The output space phasors can be classified into 4 groups: long-, medium-, short- and zero- space phasors that are depicted in black, red, blue and green respectively. The long space phasors in black are non-redundant and do not affect the neutral point. The medium space phasors in red are also non-redundant and

connect one phase of inverter to the neutral point, thus they affect the neutral point voltage and can cause its unbalance. The short space phasors in blue are redundant and come always in pairs, e.g. 18/24 generating identical line-to-line voltage. The redundancies of these space phasors can be used to control the neutral point, to redistribute losses, etc. Finally, the zero space phasor in green has three redundant states and has no impact on neutral point voltage. Due to the redundant states, only a total of 19 different line-to-line output voltages from a total 27 switching states can be synthesized by the inverter.

In the DTC scheme, the choice of the voltage space phasor to be applied to the machine is based on the value of the outputs of the torque-controller, of the stator flux-controller, and on actual sector where stator flux space phasor is located. Furthermore, a switching table that considers the influence of each voltage space phasor on the direction of movement of the flux space phasor has to be used for making the appropriate choice. If the optimum voltage space phasor to be applied to the machine is a redundant one, e.g. space phasors 15/21, an additional degree of freedom is given that can be used to control the neutral point voltage. As explained later, the selection of the appropriate redundant switching state is based on the output of the neutral point controller and on the sign of total current flowing into the neutral point of the DC-link.

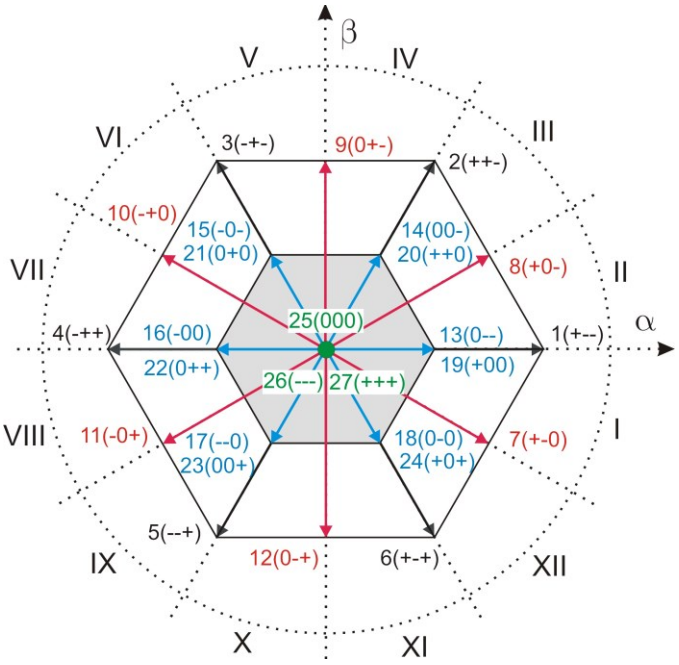

Fig. 3. Space phasor diagram of the 3L-NPC VSI

The switching table for realizing DTC with the 3L-NPC VSI is shown in TABLE I. in the appendix. The three first columns of the table correspond to the outputs of the hysteresis controllers for each variable flux, torque and neutral point voltage respectively. The sectors I to XII correspond to the location of the flux space phasor at the sampling instant according to Fig. 3.

The design of the hysteresis controllers of the DTC for multi-level voltage source inverters can be derived from the design used for two level inverters by considering the additional output voltage levels [10][11]. Thus, for an inverter with n levels, the torque controller has a characteristic that comprises *(2n-2)* hysteresis bands to deliver *(2n-1)* discrete output values [11].

Fig. 4 shows the structure of the torque controller for the 3L-NPC VSI that is used in this work. By choosing $n = 3$, the outputs *OutT*=[-2; -1; 0; +1; +2] are obtained and correspond to the second column in TABLE I. The thresholds H_{T1} and H_{T2} determine the width of the hysteresis band of torque and are set based on empirical or calculated values. For $|OutT| = 2$, the long- and medium- voltage space phasors are applied to the inverter. As mentioned above, the use of *medium* voltage space phasors has a negative impact on the control of neutral point voltage. An improvement can be achieved by avoiding the medium voltage space phasors at the expense of higher switching losses and lower current quality that in the practice is not favored. In case of $|OutT| = 1$, short voltage space phasors are employed and their redundancies can be also used to control the neutral point voltage or to redistribute the losses. Finally in the case of $OutT = 0$, the zero voltage space phasor is used and the switching state 25(000) is applied to control inverter. In order to improve the switching loss performance of the inverter, the switching states 26(---) and 27(+++) are not utilized. Obviously, when $|OutT| = 2$ or $OutT = 0$, the short voltage space phasors are not employed, thus the control of the neutral point voltage is inactive.

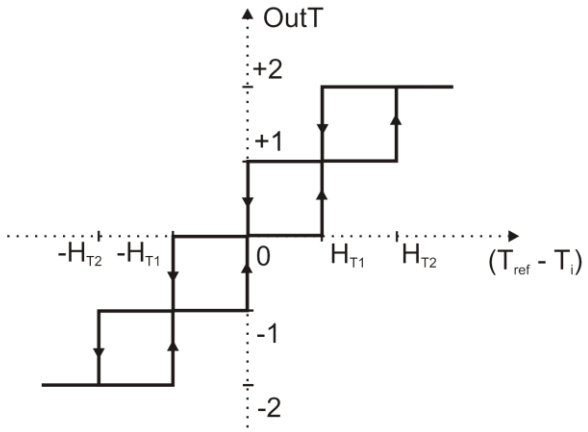

Fig. 4. Characteristic of the 5 level hysteresis torque controller

In principle the flux controller could take the same structure as for in a DTC scheme for a two level inverter, in which the flux controller has two outputs [-1;+1]. However if the same characteristic is used, the performance of the flux control becomes poor in the case of output of torque control *OutT*=0 because only the zero voltage phasors are used. To enhance the function of the flux controller, its characteristic is extended with two additional outputs [-2;+2]. In this way, the short voltage space phasors are used to reduce the flux error, although the torque controller requires the zero voltage space phasors. The ripple of the voltage of the neutral point of the DC-link is also reduced as the use of short voltage space phasors is increased. The characteristic of the flux controller is shown in Fig. 5, here the thresholds H_{F1} and H_{F2} determine the width of the hysteresis band for the amplitude of the stator flux space

phasor and the output of flux controller *OutF* corresponds to the first column of TABLE I.

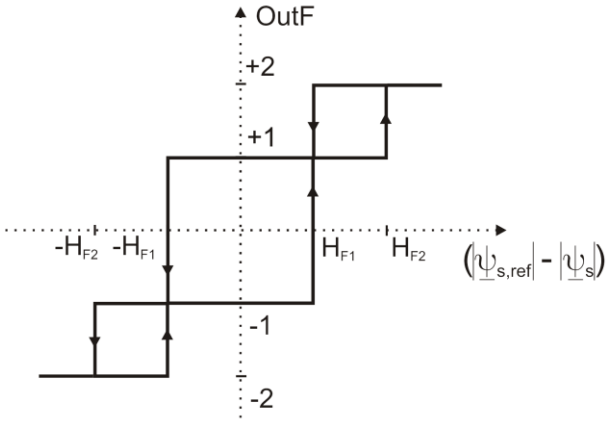

Fig. 5. Characteristic of the 4 level hysteresis stator flux controller

Fig. 6 depicts the characteristic of the 3-level hysteresis controller for the voltage of the neutral point of the DC-link. The output can take the values *OutNP* = [-1; 0; +1] and the thresholds H_{NP1} and H_{NP2} determine here the ripple of the voltage of the middle point of the DC-link.

For *OutNP* = [-1; +1] the redundancies of the space phasors have to be taken into account. For these purpose TABLE I. is used. *SignI* in the third column of the table is the sign of the total current flowing into the middle point of the DC-link, which is considered for the control of the voltage of the neutral point. The assignment of *SignI* for each short voltage space phasor is shown in TABLE III. The combined product *OutNP*·*SignI* in the third column of TABLE I. is eventually used for the proper choice of the redundant switching state of a particular short space phasor to be applied to inverter. If the output of neutral point controller $OutNP = 0$, a switching among the redundant switching states is not necessary and consequently the switching losses are reduced.

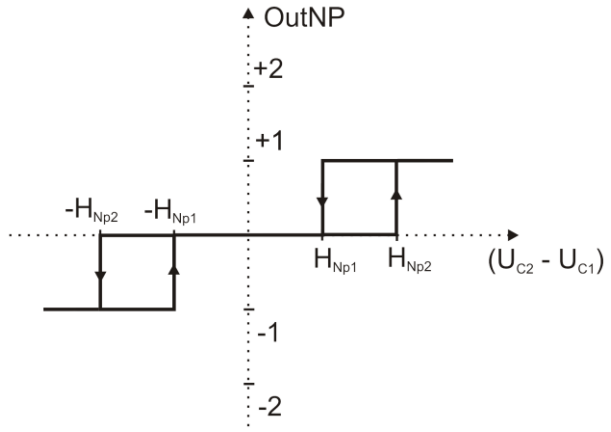

Fig. 6. Characteristic of the 3 level hysteresis controller for the voltage of the neutral point voltage $U_{NP} = U_{C1} - U_{C2}$

III. USE OF REDUNDANT STATES TO REDISTRIBUTE THE LOSSES AMONG THE DEVICE

As explained above the short voltage space phasors in the vertices of the shaded hexagon in the diagram in Fig. 3 are redundant, e.g. 18/24. For the control of the torque as well as the stator flux, it is irrelevant if the switching states e.g. 18 or 24 are used. However, their impact on the neutral point and on the loss distribution among the switches of the inverter is not the same. Usually the redundancies are used for the control of the voltage of the neutral point. In the following, the strategy for the use of the redundant states to redistribute the losses among the switches of the 3L-NPC VSI will be presented.

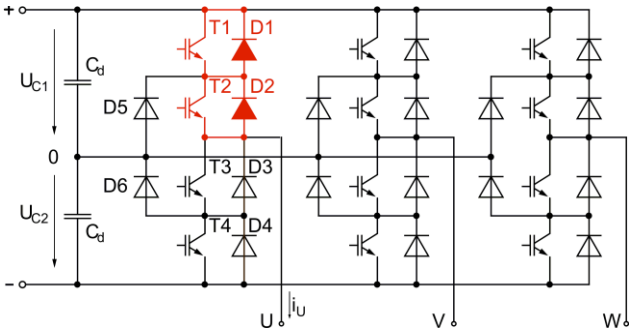

Fig. 7. 3L-NPC VSI with the neutral point voltage $U_{NP} = U_{C1} - U_{C2}$

Without loss of the generality, it can be assumed that the upper leg of phase U, switches 1 and 2 in Fig. 7, is exposed to excessive thermal load that has to be reduced in order to avoid the thermal breakdown. For the first approach, the redundant states can be used to reduce the conduction losses of IGBT 1 and 2 at the cost of higher switching losses for the same switches. The other approach is the opposite one: reduction of the switching losses at the cost of increasing the conduction losses at the same switches. As a result of extensive simulations and experimental measurements in [7][8], the second approach has proven to be the proper choice for the *high modulation index* range that is depicted as white region in Fig. 3. The ALE strategy for the *low modulation index* (shaded region in Fig. 3) has to be treated in a different way and will not be discussed in this paper.

In order to reduce the switching losses in the upper leg of phase U, the number of switching actions of this leg should be minimized by favoring those switching states, in which the upper leg of phase U remains connected to the positive DC-rail. For example with the pair (18/24) in Fig. 3; the switching state 24 ***(+0+)*** is preferred instead of the 18 ***(0-0)***, if the reduction of switching losses is aimed. Obviously, in the case examined here the use of the voltage space phasor 24 increases the conduction losses in the switches 1 and 2.

The increase of conduction losses depends mostly on the modulation index, because the duty cycle of the redundant space phasors (the short ones in the Fig. 3 spanning the inner hexagon) vary with the modulation index. The results presented later show that in spite of higher conduction losses a reduction of total losses is still achieved.

TABLE I. in the appendix shows the voltage space phasors for the control of the 3L-NPC VSI under a DTC scheme. The

highlighted fields refer to the switching states affecting the losses production on IGBT 1 and 2: highlighted in blue are the non-redundant voltage space phasors that require the connection of the upper leg of phase U to the positive DC-rail (see Fig. 7). In contrast, the short voltage space phasors that can be used to redistribute the losses from the IGBT 1 and 2 to the other switching devices are highlighted in green and are numbered as 13, 14, 18, 19, 20 and 24 (numbering rule see Fig. 3). Here, the switching states 13, 14 and 18 connect the phase U to neutral point. Conversely, the switching states 19, 20 and 24 connect phase U to positive DC bus. Thus if a thermal overload is detected in IGBT 1 or IGBT 2 , then an alternative switching table is applied to generate the switching patterns aiming at reduction of switching losses of IGBT 1 and IGBT 2. This new switching table in TABLE II. is a modification of TABLE I. , in which the switching states 13, 14 and 18 are replaced by 19, 20 and 24 respectively.

By using the modified TABLE II. the switching losses of IGBT 1 and IGBT 2 are reduced because the switching between redundant states that is used for the control of the voltage of the middle point is inhibited. Of course the drawback is the increase of the ripple.

This substitution could be carried out for all 12 sectors of the switching table. However in order to reduce the impact of the ALE strategy on the neutral point performance, the substitution is only applied in some sectors. Based on different simulation studies, it has been shown that a substitution limited to the sectors VII to XII yields the best compromise between loss reduction and ripple of neutral point voltage.

IV. CALCULATION OF THE SEMICONDUCTOR LOSSES FOR THE OPERATION UNDER ALE

A. Thermal Model

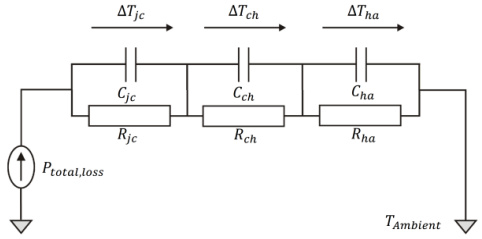

Fig. 8. Thermal model used for the calculation

Fig. 8 shows the thermal model used for the calculation of the junction temperature of the semiconductor device based on the losses. The junction temperature is given by $T_{Junction} = \Delta T_{jc} + \Delta T_{ch} + \Delta T_{ha} + T_{Ambient}$, the subscripts *jc*, *ch* and *ha* stand for *junction-to-case*, *case-to-heatsink* and *heatsink-to-ambient* temperature drop respectively. Obviously in the steady state the temperature differences are directly proportional to total losses of each semiconductor device. According to this model the temperature difference of heatsink-to-ambient ΔT_{ha} can be used to estimate the total loss of a particular IGBT including its antiparallel diode, hence $P_{total,loss} \approx \Delta T_{ha}/R_{ha}$, in steady-state. Hereby R_{ha} is the thermal resistance of the heatsink given by manufacturer.

B. Loss Calculation

For the theoretical validation of the proposed enhanced switching strategy a calculation of the losses is used. The applied method for calculating the losses of the semiconductor devices is described in [7] and was experimentally verified in [8]. It provides good accuracy with moderate calculation efforts. The conduction losses of IGBTs are calculated as:

$$P_{conduct} = U_{CE}.I_C = \left(U_{CE,0} + I_C \cdot r_{CE}\right) \cdot I_C, \quad (4)$$

I_C denotes the instant collector current through the IGBT. The Collector-Emitter voltage $U_{CE,o}$ and the differential resistance r_{CE} are extracted directly from the on-state characteristics curve. The calculation of the switching loss energy in IGBTs is formulated as:

$$E_{switch} = E_{switch,0} \cdot \frac{U_{dc}/2}{U_{base}} \cdot \frac{I_C}{I_{C,base}}, \quad (5)$$

the base switching loss $E_{switch,0}$ is obtained from the data sheet for a given condition with the base commutation voltage of U_{base} and with base collector current of $I_{C,base}$. The E_{switch} stands for either turn-on or turn-off loss energy. The average switching loss power is derived subsequently as (6), if the sample time T_{sample} of the inverter is known, typically for DTC scheme $T_{sample} = 25\mu s$.

$$P_{switch} = E_{switch}/T_{sample} \quad (6)$$

finally the overall losses are computed as the sum of all losses:

$$P = P_{conduct} + P_{switch,on} + P_{switch,off}. \quad (7)$$

In a similar manner, the conduction losses and recovery losses of the diodes are easily calculated with (4-7).

V. RESULTS

The simulation of the 3L-NPC VSI fed Induction Machine is conducted in Matlab/Simulink to examine the performance of the drive with the DTC scheme. The simulated drive system corresponds to the one used in the test-bench in the lab to verify the Active Lifetime Extension (ALE) strategy by using the PWM in the earlier works [8][9]. For the calculation of the losses, the thermal model of 3L-NPC VSI explained above and proposed in [7] was implemented in Matlab/Simulink. As already stated, this thermal model has been extensively verified by experimental measurements [8] and is considered as sufficiently accurate. The parameters of the thermal model can be obtained from the TABLE IV. as well as from the datasheets of the components. In the following, the performance of 3L-NPC VSI fed induction machine will be examined for different operational points, here the sectors VII to XII of the switching table are modified as TABLE II. (marked as red), in which the switching states 13, 14 and 18 are replaced by the 19, 20 and 24 respectively.

Fig. 9 shows the loss distribution among the IGBTs at rated operation of the induction machine, the numbering of the switches can be seen in the Fig. 7. The columns in blue refer to the conduction losses of IGBTs by applying the normal DTC scheme, columns in red refer to the conduction losses of IGBTs by applying modified DTC scheme with ALE strategy, and the grey columns on the top show the switching losses. As expected in the normal operation for the high modulation index (high speed range), the outer IGBTs, e.g. IGBT 1, produce more total losses than the inner IGBTs, e.g. IGBT 2. But by

analyzing the distribution of the conduction losses (columns in blue), the inner IGBTs causes higher conduction losses than the outer ones, because the inner IGBTs are required for both connections of one phase either to the neutral point or to the DC rail, in contrast, the outer IGBTs are required only for the connection of one phase to DC rail and have consequently shorter on-time. These results matched the experimental measurement very well and proved the sufficiency of the used thermal model of 3L-NPC VSI [7][8].

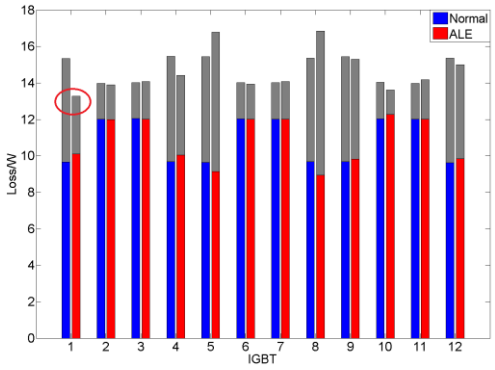

Fig. 9. Loss distribution among the IGBTs at rated operational point; the left columns refer to normal DTC and right columns to DTC with ALE.

The red columns present the conduction losses of IGBTs for DTC scheme with ALE strategy. The total losses of IGBT 1 are reduced considerably by **14%** as the losses of IGBT 2 stayed nearly the same. The IGBTs 5 and 8 suffer higher heating because of the redistribution of the losses from the IGBT 1. If the losses in IGBT 1 have to be further reduced, more sectors in TABLE I should be modified in order to decrease the switching actions of IGBT 1. Of course, this yields an additional reduction of loss on IGBT 1 but it increases at the same time the ripple at the neutral point. Consequently, the current quality becomes worse. Hence, a trade-off between ALE strategy for loss reduction and the neutral point performance has to be achieved.

The upper trace of Fig. 10 shows the waveform of neutral point voltage in normal operation. The lower trace shows the higher ripple at the neutral point due to the modification of sectors VII to XII in TABLE II. The waveforms seem to be similar to the case of applying ALE strategy with space vector modulation [7][8].

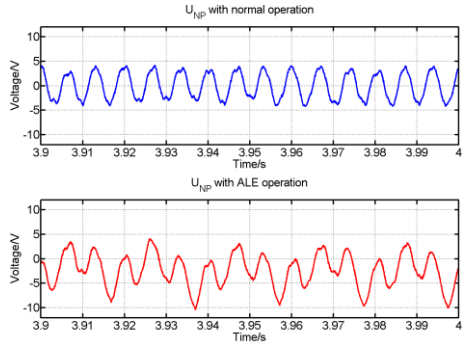

Fig. 10. Performance of neutral point for DTC with ALE at rated operation

Additionally the performance of the induction machine fed by 3L-NPC VSI was examined for different values of torque and modulation index:

$$m = \frac{U_{LL,1}}{U_{DC}/\sqrt{2}}, \tag{8}$$

Where $U_{LL,1}$ is the rms value of the fundamental of the line-to-line voltage at the output terminals of the inverter and U_{DC} is the DC-link voltage. The significant reduction of the total losses on IGBT 1 and the change of ripple of the neutral point for different operational points are shown in Fig. 11 and Fig. 12 respectively. In Fig. 11 $P_{Loss,Normal}$ are the total losses in IGBT 1 in normal DTC-operation and $P_{Loss,ALE}$ the corresponding losses in the modified DTC with ALE. The high ripple on neutral point increases the harmonic distortion in the currents, but it is acceptable as the system is working in the fault tolerant control mode to reduce the thermal overload.

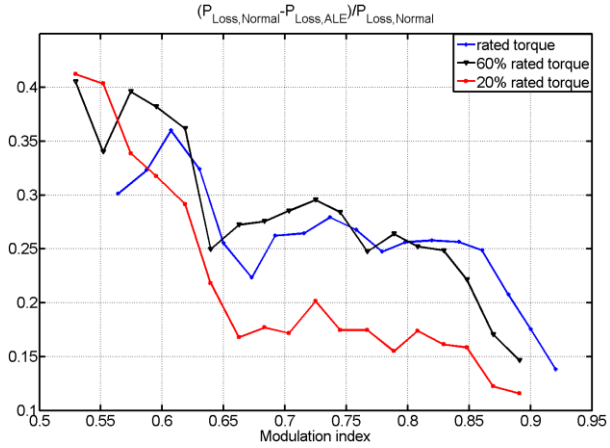

Fig. 11. Reduction of total losses on the IGBT 1

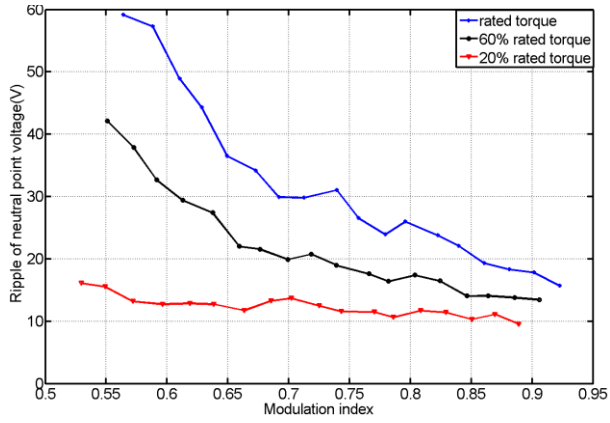

Fig. 12. Ripple of the neutral point for different operational points

VI. Conclusion

In this paper, an ALE strategy for the active loss redistribution among the switches of 3L-NPC VSI has been examined for the case of a DTC as extension to the research presented in previous works in which a field oriented control scheme and a modulator was assumed [7][8][9]. The performance of the proposed method has been examined by means of simulation

for different operational points. The performed calculations show a considerable reduction of losses at that stressed switching device while maintaining the stability of the neutral point. The ongoing work is dedicated to the verification of the method with experimental measurements.

APPENDIX

TABLE I. SWITCHING TABLE FOR 3L-NPC VSI FED INDUCTION MACHINE

OutF	OutT	OutNP *SignI	Sector I	II	III	IV	V	VI	VII	VIII	IX	X	XI	XII
+2	+2	x	2	9	3	10	4	11	5	12	6	7	1	8
	+1	+1	20	20	15	15	22	22	17	17	24	24	13	13
		-1	14	14	21	21	16	16	23	23	18	18	19	19
	0	+1	13	13	20	20	15	15	22	22	17	17	24	24
		-1	19	19	14	14	21	21	16	16	23	23	18	18
	-1	+1	24	24	13	13	20	20	15	15	22	22	17	17
		-1	18	18	19	19	14	14	21	21	16	16	23	23
	-2	x	12	6	7	1	8	2	9	3	10	4	11	5
+1	+2	x	2	9	3	10	4	11	5	12	6	7	1	8
	+1	+1	20	20	15	15	22	22	17	17	24	24	13	13
		-1	14	14	21	21	16	16	23	23	18	18	19	19
	0	+1	25											
		-1												
	-1	+1	24	24	13	13	20	20	15	15	22	22	17	17
		-1	18	18	19	19	14	14	21	21	16	16	23	23
	-2	x	12	6	7	1	8	2	9	3	10	4	11	5
-1	+2	x	9	3	10	4	11	5	12	6	7	1	8	2
	+1	+1	15	15	22	22	17	17	24	24	13	13	20	20
		-1	21	21	16	16	23	23	18	18	19	19	14	14
	0	+1	25											
		-1												
	-1	+1	17	17	24	24	13	13	20	20	15	15	22	22
		-1	23	23	18	18	19	19	14	14	21	21	16	16
	-2	x	5	12	6	7	1	8	2	9	3	10	4	11
-2	+2	x	9	3	10	4	11	5	12	6	7	1	8	2
	+1	+1	15	15	22	22	17	17	24	24	13	13	20	20
		-1	21	21	16	16	23	23	18	18	19	19	14	14
	0	+1	22	22	17	17	24	24	13	13	20	20	15	15
		-1	16	16	23	23	18	18	19	19	14	14	21	21
	-1	+1	17	17	24	24	13	13	20	20	15	15	22	22
		-1	23	23	18	18	19	19	14	14	21	21	16	16
	-2	x	5	12	6	7	1	8	2	9	3	10	4	11

The voltage space phasors in green refer to the short space phasors that have an effect on the loss production on the IGBT 1 and 2. In contrast, the ones in blue are the non-redundant space phasors. The x in column NP means that no redundant state is available, a 0 in the output of the NP controller demands no change in the output voltage.

TABLE II. MODIFIED SWITCHING TABLE FOR 3L-NPC VSI FED INDUCTION MACHINE

OutF	OutT	OutNP *SignI	Sector I	II	III	IV	V	VI	VII	VIII	IX	X	XI	XII
+2	+2	x	2	9	3	10	4	11	5	12	6	7	1	8
	+1	+1	20	20	15	15	22	22	17	17	24	24	19	19
		-1	14	14	21	21	16	16	23	23	24	24	19	19
	0	+1	13	13	20	20	15	15	22	22	17	17	24	24
		-1	19	19	14	14	21	21	16	16	23	23	24	24
	-1	+1	24	24	13	13	20	20	15	15	22	22	17	17
		-1	18	18	19	19	14	14	21	21	16	16	23	23
	-2	x	12	6	7	1	8	2	9	3	10	4	11	5
+1	+2	x	2	9	3	10	4	11	5	12	6	7	1	8
	+1	+1	20	20	15	15	22	22	17	17	24	24	19	19
		-1	14	14	21	21	16	16	23	23	24	24	19	19
	0	+1	25											
		-1												
	-1	+1	24	24	13	13	20	20	15	15	22	22	17	17
		-1	18	18	19	19	14	14	21	21	16	16	23	23
	-2	x	12	6	7	1	8	2	9	3	10	4	11	5
-1	+2	x	9	3	10	4	11	5	12	6	7	1	8	2
	+1	+1	15	15	22	22	17	17	24	24	19	19	20	20
		-1	21	21	16	16	23	23	24	24	19	19	20	20
	0	+1	25											
		-1												
	-1	+1	17	17	24	24	13	13	20	20	15	15	22	22
		-1	23	23	18	18	19	19	20	20	21	21	16	16
	-2	x	5	12	6	7	1	8	2	9	3	10	4	11
-2	+2	x	9	3	10	4	11	5	12	6	7	1	8	2
	+1	+1	15	15	22	22	17	17	24	24	19	19	20	20
	0	-1	21	21	16	16	23	23	24	24	19	19	20	20
		+1	22	22	17	17	24	24	19	19	20	20	15	15
		-1	16	16	23	23	18	18	19	19	20	20	21	21
	-1	+1	17	17	24	24	13	13	20	20	15	15	22	22
		-1	23	23	18	18	19	19	20	20	21	21	16	16
	-2	x	5	12	6	7	1	8	2	9	3	10	4	11

The voltage space phasors in green refer to the short space phasors that have an effect on the loss production on the IGBT 1 and 2. In contrast, the ones in blue are the non-redundant space phasors. The x in column NP means that no redundant state is available, a 0 in the output of the NP controller demands no change in the output voltage.

TABLE III. THE CONSIDERATION OF PHASE CURRENT FOR NEUTRAL POINT CONTROLLER

Redundant switching states	SignI
(16/22), (13/19)	$sign(I_U)$
(15/21), (18/24)	$sign(I_V)$
(14/20), (17/23)	$sign(I_W)$

TABLE IV. PARAMETERS OF THE SIMULATED SYSTEM

3L-NPC VSI	U_{DC}	560V
	C_{DC}	4,4mF
	I_{rated}	40A (rms)
Induction machine (ABB M2AA160L4)	P_{rated}	15kW
	U_{rated}	400V
	I_{rated}	31,1A
	n_{rated}	1455r/min
	M_{rated}	98 Nm
IGBT for 3L-NPC VSI (IXYS IXGR72N60A3H1)	V_{CE}	600V
	$I_{C,110}$	52A

REFERENCES

[1] Rodriguez, J.; Bernet, S.; Steimer, P.K.; Lizama, I.E.; "A Survey on Neutral-Point-Clamped Inverters," Industrial Electronics, IEEE Transactions on , vol.57, no.7, pp.2219-2230, July 2010.

[2] G. Riedel, N. Oikonomou, R. Schmidt und D. Cottet, "Active lifetime extension — Demonstrated for voltage source converters", Electrical and Electronics Engineers in Israel (IEEEI), 2010 IEEE 26th Convention of, vol., no., pp.000530-000534, 17-20 Nov. 2010.

[3] T. Bruckner, S. Bernet and H. Guldner, "The active NPC converter and its loss-balancing control".Industrial Electronics, IEEE Transactions on, vol.52, no.3, pp. 855-868, June 2005.

[4] D. Andler, J. Weber, S. Bernet and J. Rodríguez, "Improved model predictive control with loss energy awareness of a 3L-ANPC voltage source converter". Applied Electronics (AE), 2010 International Conference on, vol., no., pp.1-6, 8-9 Sept. 2010.

[5] D. Floricau, E. Floricau and G. Gateau, "Three-level active NPC converter: PWM strategies and loss distribution". Industrial Electronics, 2008. IECON 2008. 34th Annual Conference of IEEE, vol., no., pp.3333-3338, 10-13 Nov. 2008.

[6] Ke Ma; Blaabjerg, F., "Modulation Methods for Neutral-Point-Clamped Wind Power Converter Achieving Loss and Thermal Redistribution Under Low-Voltage Ride-Through," Industrial Electronics, IEEE Transactions on , vol.61, no.2, pp.835,845, Feb. 2014.

[7] The-minh Phan; Riedel, G.; Oikonomou, N.; Pacas, M., "PWM for active thermal protection in three level neutral point clamped inverters," ECCE Asia Downunder, 2013 IEEE, vol., no., pp.906-911, 3-6 June 2013.

[8] The-minh Phan; Riedel, G.; Oikonomou, N.; Pacas, M., "PWM for active thermal protection in three level neutral point clamped inverters," ECCE Pittsburgh, USA, 2014 IEEE, 14-18 September 2014.

[9] The-minh Phan; Riedel, G.; Oikonomou, N.; Pacas, M., "Active Thermal Protection and Lifetime Extension in 3L-NPC-Inverter in the low Modulation Range," APEC Charlotte, N.C., USA, 2015 IEEE, 15-19 March 2015.

[10] Buja, G.S.; Kazmierkowski, M.P., "Direct torque control of PWM inverter-fed AC motors - a survey," Industrial Electronics, IEEE Transactions on, vol.51, no.4, pp.744,757, Aug. 2004.

[11] Kieferndorf, F.; Basler, M.; Serpa, L.A.; Fabian, J.-H.; Coccia, A.; Scheuer, G.A., "A new medium voltage drive system based on ANPC-5L technology," Industrial Technology (ICIT), 2010 IEEE International Conference on , vol., no., pp.643,649, 14-17 March 2010.